Comparative Study of the Structural, Electronic, and Magnetic Properties of the Layered Ternary Vanadium Oxides CaV_4O_9, $Cs_2V_4O_9$, and $[H_2N(CH_2)_4NH_2]V_4O_9$

Yiping Zhang, Christopher J. Warren,† and Robert C. Haushalter*,†

NEC Research Institute, 4 Independence Way, Princeton, New Jersey 08540

Abraham Clearfield*

Department of Chemistry, Texas A&M University, College Station, Texas 77843

Dong-Kyun Seo and Myung-Hwan Whangbo*

Department of Chemistry, North Carolina State University, Raleigh, North Carolina 27695

Received September 30, 1997. Revised Manuscript Received January 13, 1998

We report the preparation, single-crystal X-ray structure determination, and magnetic susceptibility measurements of a new ternary vanadium oxide, $[H_2N(CH_2)_4NH_2]V_4O_9$. This compound has isolated $V_4O_9^{2-}$ layers made up of edge-sharing VO_5 square pyramids. The $V_4O_9^{2-}$ layers of $[H_2N(CH_2)_4NH_2]V_4O_9$ ($[H_2N(CH_2)_4NH_2]$ = piperidinium) differ from those of two other ternary vanadium oxides, CaV_4O_9 and $A_2V_4O_9$ (A = Rb, Cs), in the way the VO_5 square pyramids are shared, and the magnetic susceptibilities of the three oxides are widely different in their maximum susceptibility values and the temperatures where these values occur. To explain these observations, the electronic structures of the three oxides were analyzed based on molecular orbital calculations.

Introduction

The ternary vanadium oxide CaV_4O_9[1] consists of $V_4O_9^{2-}$ layers, which are made up of edge-sharing VO_5 square pyramids. The oxidation state of vanadium is +4, so each VO_5 unit contains a V^{4+} (d^1) ion. The magnetic susceptibility of this compound shows a broad maximum around 100 K and is a spin-gap system[2] (i.e., a compound having an energy gap between the magnetic ground and excited states[3]). The recently prepared vanadium oxides $A_2V_4O_9$ (A = Rb, Cs)[4] also consist of $V_4O_9^{2-}$ layers made up of edge-sharing VO_5 square pyramids. In terms of the condensation pattern of the VO_5 units, the $V_4O_9^{2-}$ layers of $A_2V_4O_9$ are different from those of CaV_4O_9, and the magnetic susceptibility of $A_2V_4O_9$ shows a broad maximum at around 600 K.[4] In the present work we report the synthesis, single crystal X-ray structure determination and magnetic susceptibility of an organically templated vanadium oxide, $[H_2N(CH_2)_4NH_2]V_4O_9$, and investigate how the structural differences in CaV_4O_9, $A_2V_4O_9$, and $[H_2N(CH_2)_4NH_2]V_4O_9$ are correlated with their magnetic susceptibility behaviors.

Experimental Section

General Methods. The chemicals used were of reagent-grade quality and were obtained from commercial sources and used without further purification. The powder X-ray diffraction patterns were obtained on a Scintag XDS 2000 diffractometer with Cu Kα radiation ($\lambda = 1.5418$ Å). The EDS analyses were performed on a Hitachi S-2700 SEM. The hydrothermal reactions were carried out in Parr acid digestion bombs with 23 mL poly(tetrafluoroethylene) liners.

Synthesis of $[H_2N(CH_2)_4NH_2]V_4O_9$. A mixture of V_2O_3 (0.130 g), piperazine (0.197 g), and H_2O (10 mL) with a mole ratio of 1.0:2.63:639 was sealed in a Parr acid digestion bomb which was heated at 170 °C for 67 h. Dark brown plates (0.122 g, yield 63% based on vanadium) were isolated after filtration, washing with water, and air-drying. A powder X-ray diffraction pattern of these crystals matched the calculated powder pattern from the single-crystal data indicating a monophasic material.

Magnetic Susceptibility Measurements. Magnetic moments for polycrystalline samples of $H_2N(CH_2)_4NH_2]V_4O_9$ were obtained using a Quantum Design SQUID magnetometer in the temperature range of 5 to 300K and at a field of 1kG.

Crystallography. A black plate having approximate dimensions of 0.12 × 0.08 × 0.02 mm was mounted on a glass fiber. All measurements were made at room temperature on a Rigaku AFC7R diffractometer with graphite-monochromated Mo Kα radiation and an 18 kW rotating anode generator. Cell constants and an orientation matrix for data collection were determined from a least-squares refinement using the setting angles of 25 carefully centered reflections in the range $22.05° < 2\theta < 25.87°$. Data were collected in the range of $5° < 2\theta < 60.1°$ using the $\omega-2\theta$ scan technique at a speed of 16°/min (in ω). The intensities of three representative reflections, which were measured after every 150 reflections, remained constant

† Present address: Symyx Technologies, 3100 Central Expressway, Santa Clara, CA 95051.

(1) Bouloux, J. C.; Galy, J. *Acta Crystallogr. Sect. B* **1973**, *29*, 1335.

(2) (a) Taniguchi, S.; Nishikawa, T.; Yasui, Y.; Kobayashi, Y.; Sato, M.; Nishioka, T.; Kontani, M.; Sano, K. *J. Phys. Soc. Jpn.* **1995**, *64*, 2758. (b) Sato, M. *Physica C* **1996**, *263*, 271. (c) Kodama, K.; Harashima, H.; Sasaki, H.; Kobayashi, Y.; Kasi, M.; Taniguchi, S.; Yasui, Y.; Sato, M.; Kakurai, K.; Mori, T.; Nishi, M. *J. Phys. Soc. Jpn.* **1997**, *66*, 793.

(3) (a) Barnes, T.; Riera, J. *Phys. Rev. B* **1994**, *50*, 6817. (b) Eccleston, R. S.; Barnes, T.; Brody, J.; Johnson, J. W. *Phys. Rev. Lett.* **1994**, *73*, 2626. (c) Azuma, M.; Hiroi, Z.; Takano, M.; Ishida, K.; Kitaoka, Y. *Phys. Rev. Lett.* **1994**, *73*, 3463. (d) Ishida, K.; Kitaoka, Y.; Asayama, K.; Azuma, M.; Hiroi, Z.; Takano, M. *J. Phys. Soc. Jpn.* **1994**, *63*, 3222.

(4) Liu, G.; Greedan, J. E. *J. Solid State Chem.* **1995**, *115*, 174.

S0897-4756(97)00653-4 CCC: $15.00
Published on Web 03/31/1998

Table 1. Crystallographic Data for $[H_2N(CH_2)_4NH_2]V_4O_9$

empirical formula	$V_4O_9N_2C_4H_{12}$
FW (g/mol)	435.91
crystal color, habit	black, plate
crystal dimensions (mm)	0.12 × 0.08 × 0.02
crystal system	monoclinic
space group	$P2_1/c$ (No. 14)
lattice parameters	$a = 5.858(2)$ Å
	$b = 16.849(5)$ Å
	$c = 11.717(3)$ Å
	$\beta = 91.21(2)°$
	$V = 1156.2(5)$ Å^3
Z	4
D_{calc} (g·cm^{-3})	2.504
μ Mo Kα (cm^{-1})	24.74
diffractometer	Rigaku AFC7R
scan type	$\omega-2\theta$
2θ max	60.1°
obsd reflections ($I > 3.00\sigma(I)$)	1742
no. of variables	172
R; R_w[a]	0.035; 0.040
goodness of fit	1.81
max/min peak in final diff map (e$^-$/Å^3)	0.86/−0.53

[a] $R = \sum||F_o| - |F_c||/\sum|F_o|$; $R_w = (\sum w(|F_o| - |Fc|)^2/\sum wF_o^2)^{1/2}$.

throughout data collection. Of the 3172 reflections that were collected, 2871 were unique ($R_{int} = 0.048$). Empirical absorption corrections based on ψ-scan measurements were applied. The data were corrected for Lorentz and polarization effects. The structure was solved by direct methods. All non-hydrogen atoms in the structure were refined anisotropically. The hydrogen atoms were located from difference Fourier maps and included in the refinement with fixed positional and thermal parameters. The final cycle of full-matrix least-squares refinement was based on 1742 observed reflections with $I \geq 3\sigma(I)$ and 172 variable parameters. The maximum and minimum peaks on the final difference Fourier map corresponded to 0.86 and −0.53 e$^-$/Å^3. Neutral atom scattering factors were taken from Cromer and Waber.[5] Anomalous dispersion effects were included and the values for $\Delta f'$ and $\Delta f''$ were those of Creagh and McAuley.[6] All calculations were performed using the *teXsan* crystallographic software package of Molecular Structure Corp.[7] Further details of the crystallographic investigation of $[H_2N(CH_2)_4NH_2]V_4O_9$ are listed in Table 1, positional and thermal parameters of the atoms in the structure are given in Table 2, and selected bond distances and angles are given in Table 3.

Results and Discussion

As can be seen in Figure 1, the structure of $[H_2N(CH_2)_4NH_2]V_4O_9$ consists of vanadium oxide layers with protonated piperazine dications occupying the interlamellar space. A view perpendicular to the oxide layer is shown in Figure 2. The layers with a composition of $[V_4O_9]^{2-}$ are composed of corner- and edge-sharing VO_5 square pyramids. There are four V atoms in the structure that are crystallographically independent. Each of them has a square-pyramidal coordination environment with the apical oxygen at a distance of around 1.62 Å and four basal oxygens at distances in the range of 1.917 (4)−2.054 (4) Å. The assignment of oxidation state of +4 to all the V atoms is consistent with their coordination configurations and is confirmed by bond valence sum calculations.[8] The oxide layer consists of groups of four VO_5 square pyramids that are connected together by sharing two edges with each other. Each group of four square pyramids is then connected to four neighboring groups via edge-sharing in such a way that eight-member rings are formed. Each of the eight-member rings has a square-planar-like shape and

Table 2. Positional Parameters and *B*(eq) for $[H_2N(CH_2)_4NH_2]V_4O_9$

atom	x	y	z	B(eq)[a]
V(1)	0.0280(2)	0.29686(5)	0.33800(7)	0.68(2)
V(2)	0.1968(2)	0.22443(5)	0.12377(8)	0.68(2)
V(3)	−0.3720(2)	0.30079(5)	0.21642(8)	0.74(2)
V(4)	0.4567(2)	0.21499(5)	0.42502(7)	0.73(2)
O(1)	0.0644(7)	0.3905(2)	0.3645(3)	1.36(8)
O(2)	−0.0584(3)	0.2827(2)	0.1799(3)	0.89(8)
O(3)	0.3267(7)	0.2564(2)	0.2763(3)	0.96(7)
O(4)	0.1410(6)	0.2341(2)	0.4687(3)	0.74(7)
O(5)	0.1433(7)	0.1299(2)	0.1271(4)	1.64(9)
O(6)	−0.4037(7)	0.3959(2)	0.2036(3)	1.44(9)
O(7)	−0.4934(7)	0.2493(2)	0.0810(3)	0.98(8)
O(8)	−0.2815(7)	0.2721(2)	0.3690(3)	1.25(8)
O(9)	0.5040(7)	0.1202(2)	0.4194(4)	1.71(9)
N(1)	0.0374(9)	0.5843(3)	−0.0033(4)	1.4(1)
N(2)	0.338(1)	0.5147(3)	0.5858(5)	2.9(1)
C(1)	0.012(1)	0.5417(3)	0.1077(5)	1.6(1)
C(2)	−0.093(1)	0.5437(3)	−0.0958(5)	1.7(1)
C(3)	0.348(1)	0.5656(4)	0.4811(8)	3.4(2)
C(4)	0.438(1)	0.5024(5)	0.3840(7)	3.3(2)

[a] $B(eq) = {}^8/_3\pi^2(U_{11}(aa^*)^2 + U_{22}(bb^*)^2 + U_{33}(cc^*)^2 + 2U_{12}aa^*bb^* \cos\gamma + 2U_{13}aa^*cc^* \cos\beta + 2U_{23}bb^*cc^* \cos\alpha)$.

Table 3. Selected Bond Distances (Å) and Angles (deg) in $[H_2N(CH_2)_4NH_2]V_4O_9$

Bond Distances			
V(1)−O(1)	1.622(4)	V(1)−O(2)	1.924(4)
V(1)−O(3)	2.025(4)	V(1)−O(4)	1.965(4)
V(1)−O(8)	1.903(4)	V(2)−O(2)	1.917(4)
V(2)−O(3)	2.002(4)	V(2)−O(4)	1.967(4)
V(2)−O(5)	1.623(4)	V(2)−O(7)	1.931(4)
V(3)−O(2)	1.919(4)	V(3)−O(3)	2.054(4)
V(3)−O(6)	1.620(4)	V(3)−O(7)	1.931(4)
V(3)−O(8)	1.916(4)	V(4)−O(3)	2.012(4)
V(4)−O(4)	1.956(4)	V(4)−O(7)	1.940(4)
V(4)−O(8)	1.936(4)	V(4)−O(9)	1.622(4)
N(1)−C(1)	1.495(7)	N(1)−C(2)	1.481(8)
N(2)−C(3)	1.499(10)	N(2)−C(4)	1.476(10)
C(1)−C(2)	1.523(8)	C(3)−C(4)	1.48(1)
Bond Angles			
O(1)−V(1)−O(2)	109.6(2)	O(1)−V(1)−O(3)	106.5(2)
O(1)−V(1)−O(4)	109.5(2)	O(1)−V(1)−O(8)	107.4(2)
O(2)−V(1)−O(3)	80.0(2)	O(2)−V(1)−O(4)	139.6(2)
O(2)−V(1)−O(8)	85.7(2)	O(3)−V(1)−O(4)	79.5(2)
O(3)−V(1)−O(8)	145.9(2)	O(4)−V(1)−O(8)	92.3(2)
O(2)−V(2)−O(3)	80.8(2)	O(2)−V(2)−O(4)	91.1(2)
O(2)−V(2)−O(5)	110.0(2)	O(2)−V(2)−O(7)	136.0(2)
O(3)−V(2)−O(4)	141.4(2)	O(3)−V(2)−O(5)	108.2(2)
O(3)−V(2)−O(7)	80.4(2)	O(4)−V(2)−O(5)	110.0(2)
O(4)−V(2)−O(7)	79.8(2)	O(5)−V(2)−O(7)	113.6(2)
O(2)−V(3)−O(3)	148.4(2)	O(2)−V(3)−O(6)	104.2(2)
O(2)−V(3)−O(7)	94.8(2)	O(2)−V(3)−O(8)	85.5(2)
O(3)−V(3)−O(6)	107.1(2)	O(3)−V(3)−O(7)	79.2(2)
O(3)−V(3)−O(8)	79.2(2)	O(6)−V(3)−O(7)	109.2(2)
O(6)−V(3)−O(8)	111.4(2)	O(7)−V(3)−O(8)	138.0(2)
O(3)−V(4)−O(4)	80.0(2)	O(3)−V(4)−O(7)	139.0(2)
O(3)−V(4)−O(8)	79.8(2)	O(3)−V(4)−O(9)	111.6(2)
O(4)−V(4)−O(7)	80.0(2)	O(4)−V(4)−O(8)	140.1(2)
O(4)−V(4)−O(9)	109.6(2)	O(7)−V(4)−O(8)	93.5(2)
O(7)−V(4)−O(9)	108.7(2)	O(8)−V(4)−O(9)	109.8(2)
C(1)−N(1)−C(2)	110.8(4)	C(3)−N(2)−C(4)	111.9(6)
N(1)−C(1)−C(2)	109.7(5)	N(1)−C(2)−C(1)	110.3(5)
N(2)−C(3)−C(4)	110.9(6)	N(2)−C(4)−C(3)	110.6(6)

(5) Cromer, D. T.; Waber, J. T. *International Tables for X-ray Crystallography*; Kynoch Press: Birmingham, U.K., 1974; Vol. IV, Table 2.2A.

(6) Creagh, D. C.; McAuley, W. J. *International Tables for Crystallography*; Wilson, A. J. C., Ed.; Kluwer Academic Publishers: Boston, 1992; Vol. C, Table 4.2.4.3, pp 200−206.

(7) teXsan: *Texray Structural Analysis Package*; Molecular Structure Corporation, The Woodlands, TX, 1995, Version 1.7-1.

(8) Brown, I. D.; Altermatt, D. *Acta Crystallogr.* **1985**, *B41*, 244.

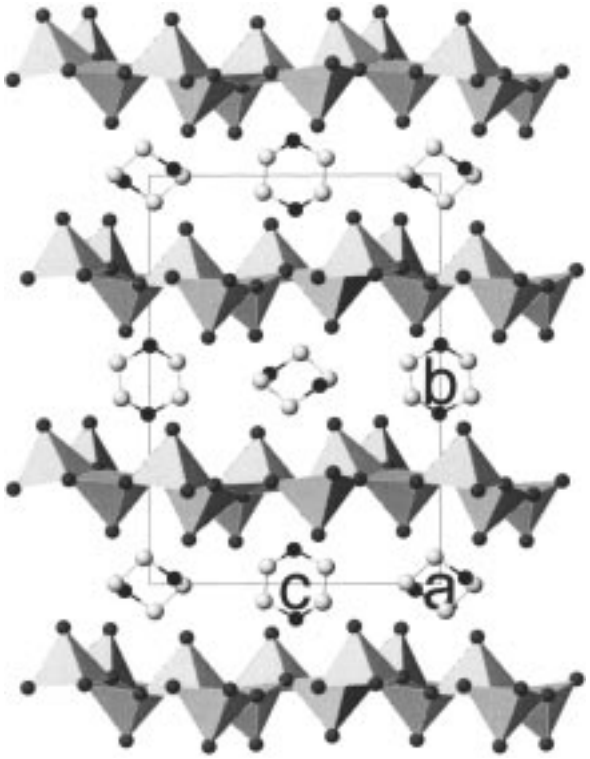

Figure 1. View of the structure of $[H_2N(CH_2)_4NH_2]V_4O_9$ down the crystallographic *a* axis showing the layers of vanadium oxide (polyhedra) and piperazine dications (ball-and-stick) in the interlayer space.

consists of four oxygens and four vanadium atoms. The piperazine molecules between the oxide layers are protonated and form extensive hydrogen bonds with the oxide layers.

Comparison of the $V_4O_9^{2-}$ Layers of CaV_4O_9, $Cs_2V_4O_9$, and $[H_2N(CH_2)_4NH_2]V_4O_9$. The $V_4O_9^{2-}$ layers of CaV_4O_9, $Cs_2V_4O_9$, and $[H_2N(CH_2)_4NH_2]V_4O_9$ are composed of edge-sharing VO_5 square pyramids. The VO_5 pyramids of the three $V_4O_9^{2-}$ layers have similar structures; the $V-O_a$ and $V-O_b$ distances are about 1.6

and 1.9−2.0 Å, respectively, where O_a and O_b are the apical and basal oxygen atoms of a VO_5 pyramid. The VO_5 square pyramids having the axial oxygen atoms pointed above and below the basal plane can be represented by the projection views a and b, respectively.

Accordingly, the $V_4O_9^{2-}$ layers of CaV_4O_9, $Cs_2V_4O_9$, and $[H_2N(CH_2)_4NH_2]V_4O_9$ (**1**) possess the edge-sharing patterns shown in Figure 3a−c, respectively. The magnetic susceptibility vs temperature (χ vs T) plot determined for $[H_2N(CH_2)_4NH_2]V_4O_9$ is presented in Figure 4. For the purpose of comparison, the χ vs T plots for CaV_4O_9[2] and $A_2V_4O_9$ (A = Rb, Cs)[4] are shown in Figures 5 and 6, respectively. As can be seen in the figures, each χ vs T plot exhibits a broad maximum, thereby indicating the occurrence of antiferromagnetic interactions between spins. The three compounds have different maximum χ values (χ_{max}) at different temperatures (T_{max}): $\chi_{max} = 0.0011$ emu/mol and $T_{max} = 560$ K for $Cs_2V_4O_9$, $\chi_{max} = 0.0028$ emu/mol and $T_{max} = 100$ K for CaV_4O_9, and $\chi_{max} = 0.011$ emu/mol and $T_{max} = 30$ K for $[H_2N(CH_2)_4NH_2]V_4O_9$. In general, the higher T_{max}

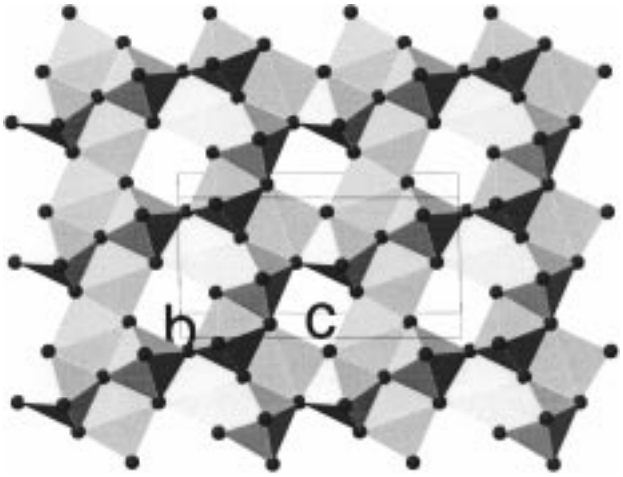

Figure 2. View perpendicular to the vanadium oxide layer in the structure of $[H_2N(CH_2)_4NH_2]V_4O_9$.

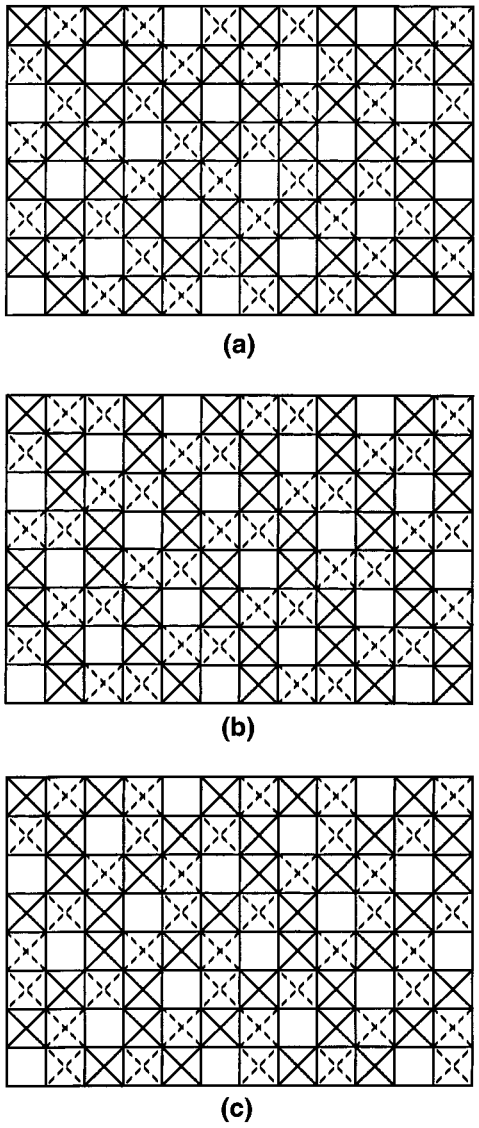

Figure 3. Schematic projection views of the $V_4O_9^{2-}$ layers of (a) CaV_4O_9, (b) $Cs_2V_4O_9$, and (c) $[H_2N(CH_2)_4NH_2]V_4O_9$.

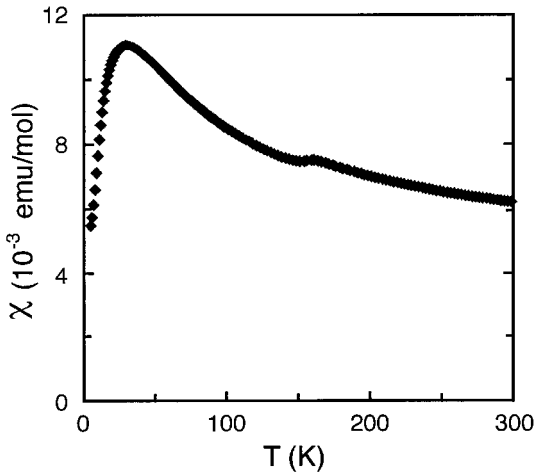

Figure 4. Magnetic susceptibility vs temperature plot determined for $[H_2N(CH_2)_4NH_2]V_4O_9$.

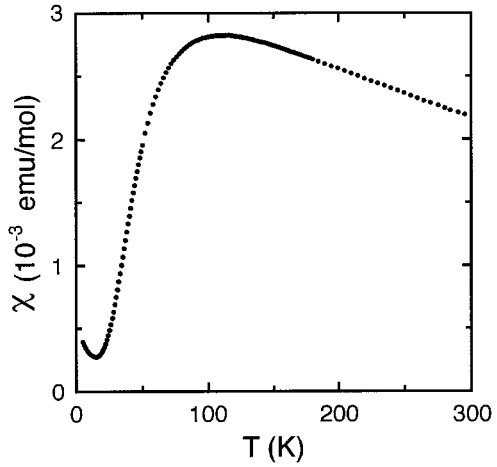

Figure 5. Magnetic susceptibility vs temperature plot determined for CaV_4O_9 (adapted from ref 2).

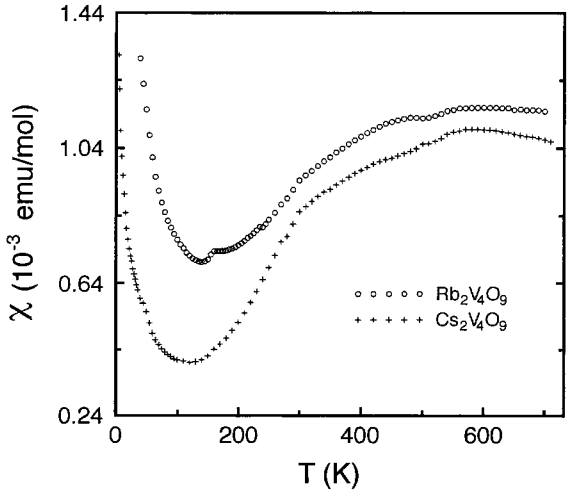

Figure 6. Magnetic susceptibility vs temperature plot determined for $A_2V_4O_9$ (A = Rb, Cs) (adapted from ref 4).

value (or the lower χ_{max} value) signifies the larger magnetic excitation energy. Therefore, the most strongly coupled spins are present in $Cs_2V_4O_9$, while the most weakly coupled spins are present in $[H_2N(CH_2)_4NH_2]V_4O_9$. In the χ vs T plot of $[H_2N(CH_2)_4NH_2]V_4O_9$, the decrease of χ in the temperature region above T_{max} is not sharp. The latter suggests that $[H_2N(CH_2)_4NH_2]V_4O_9$ also has more strongly coupled spins, the magnetic excitation energies of which become accessible at temperatures above T_{max}.

Electronic Structure and Antiferromagnetic Interaction. It is of importance to explore how the different magnetic properties of CaV_4O_9, $Cs_2V_4O_9$, and $[H_2N(CH_2)_4NH_2]V_4O_9$ are related to the structures of their $V_4O_9^{2-}$ layers. Each VO_5 square pyramid contains one unpaired d-electron. To describe the interactions between these electrons, it is necessary to discuss the structures of the $V_4O_9^{2-}$ layers from the viewpoint of whether adjacent VO_5 pyramids have a trans or cis arrangement as represented below:

trans cis

For simplicity, the V^{4+} ion of each VO_5 square pyramid may be represented by a node, and the cis and trans arrangements between adjacent V^{4+} ion centers by thin and thick lines, respectively. Then, the $V_4O_9^{2-}$ layers of CaV_4O_9, $Cs_2V_4O_9$, and $[H_2N(CH_2)_4NH_2]V_4O_9$ exhibit the patterns of the cis and trans arrangements shown in Figure 7a−c, respectively. In all the $V_4O_9^{2-}$ layers, each V^{4+} center interacts with three adjacent V^{4+} centers through the shared O−O edges. The adjacent VO_5 pyramids of the $V_4O_9^{2-}$ layers have only trans arrangements in CaV_4O_9 but both cis and trans arrangements in $Cs_2V_4O_9$ and $[H_2N(CH_2)_4NH_2]V_4O_9$. For simplicity, the interactions between adjacent spin centers via the cis and trans arrangements may be referred to as the cis and trans interactions, respectively. Then, each spin has three trans interactions in CaV_4O_9 (Figure 7a) and one cis and two trans interactions in $A_2V_4O_9$ (Figure 7b). In $[H_2N(CH_2)_4NH_2]V_4O_9$, there are two kinds of spins; one having three trans interactions and the other having one cis and two trans interactions (Figure 7c). The condensation patterns of Figures 7a−c may also be described in terms of tetramer units as shown below:

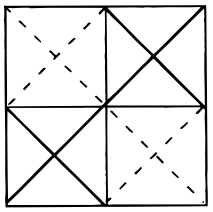

tetramer unit

Within a tetramer unit, every edge-sharing dimer has a trans interaction. Adjacent tetramer units have only trans interactions in CaV_4O_9, only cis interactions in $A_2V_4O_9$, and cis and trans interactions in $[H_2N(CH_2)_4NH_2]V_4O_9$. Our discussion considers only those metal−metal interactions occurring through shared O−O edges and neglects those occurring through shared oxygen corners. This approximation is justified because the former are much stronger in magnitude than the latter.[9]

The exchange coupling constant, J, between two adjacent spins can be written as $J = J_F + J_{AF}$, where J_F and J_{AF} refer to the ferromagnetic and antiferromag-

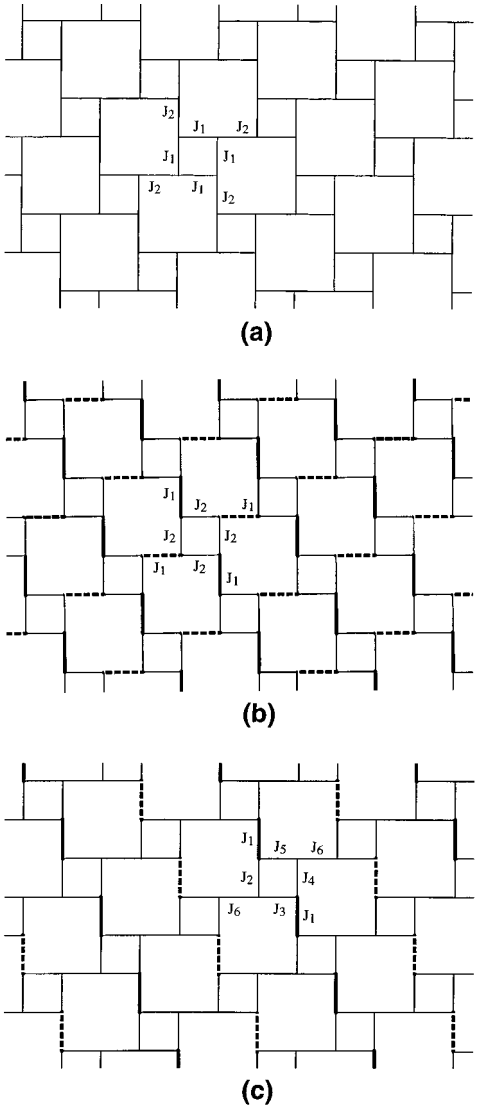

Figure 7. Patterns for the cis and trans interactions in the $V_4O_9^{2-}$ layers of (a) CaV_4O_9, (b) $Cs_2V_4O_9$, and (c) $[H_2N(CH_2)_4NH_2]V_4O_9$. The cis dimers with apical oxygen atoms pointed above and below the layer are represented by solid and dashed lines, respectively.

netic interactions. For antiferromagnetic systems, J_F is negligible so that $J \approx J_{AF}$.[10] (For simplicity, J_{AF} is simply represented by J in the remainder of our discussion.) To a first approximation, the strength of a cis or trans interaction (i.e., the magnitude of J) is proportional to the square of the energy difference (ΔE, see below) between the highest two singly filled levels of the cis or trans dimer $V_2O_8^{8-}$ (i.e., $J_{AF} \propto \Delta E^2$), respectively.[10,11]

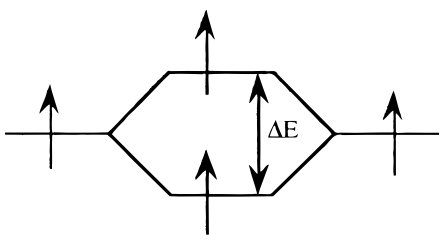

We calculate the ΔE values for various possible cis- and trans- $V_2O_8^{8-}$ dimers of the $V_4O_9^{2-}$ layers on the basis of the extended Hückel method.[12]

For the $V_4O_9^{2-}$ layer of $Cs_2V_4O_9$ (Figure 7b), the J value of the cis dimer is calculated to be much larger than that of the trans dimer (i.e., $\Delta E_1 = 0.746$ eV, $\Delta E_2 = 0.104$ eV, and $J_2/J_1 = 0.019$). Thus, the spins are strongly coupled in each cis dimer unit, and their interactions via the trans arrangements are weak. This explains why the χ_{max} value is small, and T_{max} is high. If spin dimers are completely isolated, the T_{max} is related to J through[10]

$$|J|/k_B T_{max} = 1.599 \quad (1)$$

and the magnetic susceptibility, χ, is decreased by[10]

$$\chi = 2Ng^2\beta^2/k_B T[3 + \exp(-J/k_B T)] \quad (2)$$

Given that $T_{max} = 560$ K, eqs 1 and 2 lead to $\chi_{max} = 0.67 \times 10^{-3}$ emu/mol, which is considerably smaller than the observed value of 1.10×10^{-3} emu/mol. Therefore, adjacent cis dimers of $Ca_2V_4O_9$ do interact substantially via trans arrangements.

As already mentioned, there are two kinds of spin centers in the $V_4O_9^{2-}$ layer of $[H_2N(CH_2)_4NH_2]V_4O_9$ (Figure 7c). By analogy with the above analysis, it is reasonable to consider that the unpaired spins in each cis dimer are strongly coupled ($\Delta E_1 = 0.955$ eV), and their interactions via trans arrangements are weak ($\Delta E_2 = 0.194$ eV, $\Delta E_3 = 0.214$, $\Delta E_4 = 0.201$ eV, and $\Delta E_5 = 0.104$ eV). Then, the spins engaged in three trans interactions are left over to interact between them ($\Delta E_6 = 0.280$ eV), which constitute trans dimers. To a first approximation, therefore, one may attempt to describe the magnetic susceptibility of $[H_2N(CH_2)_4NH_2]V_4O_9$ in terms of cis and trans dimers. Suppose that $[H_2N(CH_2)_4NH_2]V_4O_9$ consists of isolated spin dimers. Then from the fact that $T_{max} = 30$ K, eqs 1 and 2 lead to $\chi_{max} = 0.012$ emu/mol, which is very close to the observed value of 0.011 emu/mol, and to $\chi = 2.4 \times 10^{-3}$ emu/mol at 300 K, which is considerably smaller than the experimental value of 6.3×10^{-3} emu/mol. Consequently, the magnetic susceptibility at low temperatures around T_{max} is well described in terms of isolated spin dimers. According to our molecular orbital calculations, these spin dimers are identified as the trans dimers, which have the lower ΔE than do the cis dimers (i.e., $\Delta E_6 = 0.288$ eV vs $\Delta E_1 = 0.955$ eV, which amounts to $J_6/J_1 = 0.12$). In short, the susceptibility at low temperatures around T_{max} is well described in terms of almost noninteracting trans dimers. The susceptibility at high temperatures above T_{max} should be described in terms of both trans and cis dimers and their interactions. The latter explains the slow decrease in χ above T_{max}.

Consequently, the essential difference between the magnetic susceptibilities of $[H_2N(CH_2)_4NH_2]V_4O_9$ and $Cs_2V_4O_9$ can be described in terms of the schematic energy diagrams shown in Figure 8. $[H_2N(CH_2)_4NH_2]V_4O_9$ has trans and cis dimers as spin centers, while $Cs_2V_4O_9$ has only cis dimers as spin centers. Our molecular orbital calculations show that spins of the cis

(9) Candell, E.; Whangbo, M.-H. Chem. Rev. **1991**, *91*, 965.
(10) Kahn, O. *Molecular Magnetism*; VCH Publishers: Weinheim, 1993, Chapter 8.
(11) Hay, P. J.; Thibeault, J. C.; Hoffmann, R. *J. Am. Chem. Soc.* **1975**, *97*, 4884.
(12) Hoffmann, R. *J. Chem. Phys.* **1963**, *39*, 1397.

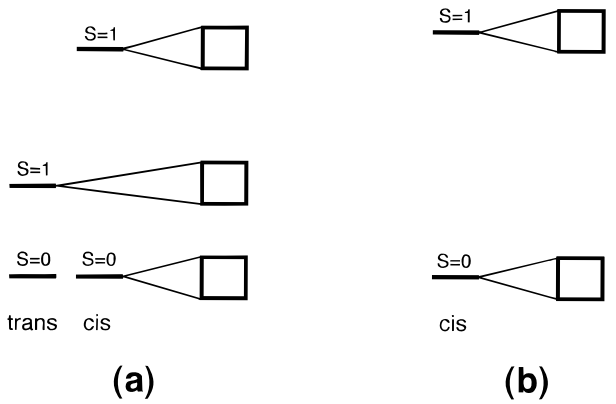

Figure 8. Schematic diagrams of the low-lying magnetic energy levels of (a) $[H_2N(CH_2)_4NH_2]V_4O_9$ and (b) $Cs_2V_4O_9$. The discrete energy levels refer to the trans and cis dimers in (a), and the cis dimer in (b). Interactions between dimers make the discrete energy levels spread into bands.

dimers interact more strongly than those of the trans dimers. Therefore, the low-lying magnetic energy levels of $[H_2N(CH_2)_4NH_2]V_4O_9$ are schematically represented by Figure 8a, and those of $Cs_2V_4O_9$ by Figure 8b. $[H_2N(CH_2)_4NH_2]V_4O_9$ provides low-lying excited states that are accessible at low temperatures because it has trans dimers. Such excited states are not available for $Cs_2V_4O_9$ because it does not have trans dimers.

For the $V_4O_9^{2-}$ layer of CaV_4O_9 (Figure 7a), the J values are calculated to be similar (i.e., $\Delta E_1 = 0.307$ eV, $\Delta E_2 = 0.298$ eV, and $J_2/J_1 = 0.94$). The compound CaV_4O_9 is therefore a spin-gap system, with energy gap $\Delta = 74$ cm^{-1}.[2] We now estimate the J values by considering the magnetic states expected for the four spins of an isolated tetramer. The four spin centers may be labeled as shown in the tetramer unit below:

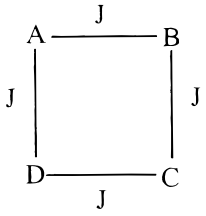

As already pointed out, the interaction between A and C or between B and D can be neglected because it occurs through a shared corner rather than through a shared edge. Then, the spin Hamiltonian for the above system can be written as

$$H = -J(S_A \cdot S_B + S_B \cdot S_C + S_C \cdot S_D + S_D \cdot S_A) = -J(S^2 - S'^2 - S''^2)/2 \quad (3)$$

where $S = S_A + S_B + S_C + S_D$, $S' = S_A + S_C$, and $S'' = S_B + S_D$. The eigenvalues of this Hamiltonian are given by

$$E(S,S',S'') = -J[S(S+1) - S'(S'+1) - S''(S''+1)]/2 \quad (4)$$

where $S = 0, 1, 2$; $S' = 0, 1$; and $S'' = 0, 1$. Thus, the first excitation energy is $2|J|$. When the tetramer units in the two-dimensional lattice (Figure 7a) interact, each magnetic energy level given by eq 4 is spread into a band. Therefore, the first excitation energy of the lattice (i.e., the spin gap Δ) should be smaller than $2|J|$ (i.e., $|J| > \Delta/2$). This provides the estimate that $|J| > 37$ cm^{-1}.

Concluding Remarks

The ternary oxides CaV_4O_9, $A_2V_4O_9$ (A = Rb, Cs), and $[H_2N(CH_2)_4NH_2]V_4O_9$ all consist of $V_4O_9^{2-}$ layers made up of edge-sharing VO_5 square pyramids. The $V_4O_9^{2-}$ layers of these oxides are different in the way the VO_5 pyramids are condensed, and as a result their magnetic susceptibilities are different. The adjacent VO_5 pyramids of the $V_4O_9^{2-}$ layers have only trans arrangements in CaV_4O_9, but both cis and trans arrangements in $Cs_2V_4O_9$ and $[H_2N(CH_2)_4NH_2]V_4O_9$. The differences in the magnetic properties of the three oxides are explained in terms of the cis and trans interactions between adjacent spins. Our MO calculations of various cis and trans dimers, $V_2O_8^{8-}$, show that the spin-exchange coupling constant for a cis interaction is much larger in magnitude than that for a trans interaction. The compounds $A_2V_4O_9$ show the magnetic susceptibility expected for systems consisting of weakly interacting strongly coupled spin dimers (i.e., cis dimers). The compound $[H_2N(CH_2)_4NH_2]V_4O_9$ exhibits the magnetic susceptibility expected for a system consisting of two kinds of weakly interacting spin dimers (i.e., trans and cis dimers). The magnetic susceptibility at low temperatures around T_{max} originates mainly from the trans dimers, and that at high temperatures above T_{max} from both trans and cis dimers. The $V_4O_9^{2-}$ layer of CaV_4O_9 has no cis interaction, so there is no strongly coupled spin dimer. The consideration of the magnetic states of a tetramer and the spin gap lead to the estimate of the magnitude of the spin exchange coupling constant, $|J| > 37$ cm^{-1}.

Acknowledgment. The work at Texas A&M University was supported by the National Science Foundation under Grant DMR-9107715. The work at North Carolina State University was supported by the U.S. Department of Energy, Office of Basic Sciences, Division of Materials Sciences, under Grant DE-FG05-86ER45259.

Supporting Information Available: Complete tables of crystallographic conditions, atomic positional parameters, bond lengths and angles, and anisotropic temperature factors for $[H_2N(CH_2)_4NH_2]V_4O_9$ (13 pages); observed and calculated structure factors (12 pages). Ordering information is given on any current masthead page.

CM970653N